J. Fluid Mech. (2009), *vol.* 623, *pp.* 167–185.
doi:10.1017/S0022112008005260 Printed in the United Kingdom

Analysis of the unstable Tollmien–Schlichting mode on bodies with a rounded leading edge using the parabolized stability equation

M. R. TURNER† AND P. W. HAMMERTON
School of Mathematics, University of East Anglia, Norwich NR4 7TJ, UK

(Received 21 December 2007 and in revised form 5 November 2008)

The interaction between free-stream disturbances and the boundary layer on a body with a rounded leading edge is considered in this paper. A method which incorporates calculations using the parabolized stability equation in the Orr–Sommerfeld region, along with an upstream boundary condition derived from asymptotic theory in the vicinity of the leading edge, is generalized to bodies with an inviscid slip velocity which tends to a constant far downstream. We present results for the position of the lower branch neutral stability point and the magnitude of the unstable Tollmien–Schlichting (T-S) mode at this point for both a parabolic body and the Rankine body. For the Rankine body, which has an adverse pressure gradient along its surface far from the nose, we find a double maximum in the T-S wave amplitude for sufficiently large Reynolds numbers.

1. Introduction

When a body is placed in a mean flow with a small-amplitude unsteady perturbation, the position of boundary layer transition depends on the stability characteristics of the body and the interactions of the unsteady disturbance with the boundary layer, a process known as receptivity (Morkovin 1985). For two-dimensional large Reynolds number flows, the transfer of energy from the free-stream disturbance to the instability wave occurs due to non-parallel mean flow effects. These effects occur at the leading edge of the body (Goldstein 1983) or further downstream where the mean flow varies rapidly in the streamwise direction, such as at surface roughness elements (Goldstein 1985; Kerschen, Choudhari & Heinrich 1990), regions of marginal stability (Goldstein, Leib & Cowley 1992) or changes in surface roughness (Goldstein & Hultgren 1989). Once energy has been transferred to this instability wave, the disturbance typically decays in amplitude downstream until the lower branch neutral stability point is reached, beyond which the disturbance grows until nonlinear effects become important and transition occurs. The work by Saric, Reed & Kerschen (2002) reviews the asymptotic, numerical and experimental approaches to receptivity and transition.

In this paper we formulate a general theory for calculating the position of the lower branch neutral stability point and the amplitude of the instability wave at this point for bodies where the slip velocity tends to a constant far downstream. Using

† Present address for correspondence: Mathematics Research Institute, School of Engineering, Computing and Mathematics, University of Exeter, Exeter EX4 4QF, UK. Email: M.R.Turner@ex.ac.uk.

this theory we make a comparison of the results for a parabolic body, which has a positive pressure gradient along its surface, and a Rankine body, which has a negative pressure gradient along the majority of its surface. The qualitative behaviour of these two bodies along with the flat plate considered in Turner & Hammerton (2006) covers bodies with a positive, a negative and a zero-pressure gradient on its surface.

For small-amplitude unsteady disturbances to a semi-infinite flat plate, Goldstein (1983) calculates the asymptotic structure along the plate for large Reynolds numbers. This asymptotic structure consists of a region close to the leading edge where the flow is governed by the unsteady boundary layer equation. The far downstream asymptotic form of the solution in this region consists of a Stokes layer and a sum of asymptotic eigenmodes (Lam & Rott 1960, 1993) which, through a multiplicative receptivity coefficient, links the amplitude of these eigenmodes to the free-stream disturbance. As we move downstream of the leading edge, the linearized unsteady boundary layer equation (LUBLE) breaks down but it can be asymptotically matched to the large-Reynolds-number, small wavenumber form of the classical Orr–Sommerfeld equation. It is also shown that the first of the Lam–Rott eigenmodes matches to the unstable Tollmien–Schlichting (T-S) mode of the Orr–Sommerfeld equation. In this Orr–Sommerfeld region for the semi-infinite flat plate there exists asymptotic solutions to the two-dimensional Navier–Stokes equations which represent two-dimensional T-S eigenmodes at the lower orders of approximation and eventually account for the weak non-parallel flow effects at the higher orders (Smith 1979). This will yield expressions for both the growth rate and the mode shape of these eigenmodes. However, this asymptotic expansion becomes non-uniform downstream when the work of Goldstein (1982) is considered, and so cannot be used to calculate the amplitude of the unstable T-S mode at the lower branch neutral stability point (Turner 2007). This non-uniformity is not apparent in the work of Smith (1979), and is an ongoing topic of study.

Numerous numerical studies have calculated growth rates of the T-S modes in the Orr–Sommerfeld region on a semi-infinite flat plate. The simplest methods use just the Orr–Sommerfeld equation, but this approach neglects the streamwise growth of the boundary layer. The non-parallel effects can be incorporated into this equation by considering an asymptotic expansion in powers of $Re^{-1/2}$, where Re is the Reynolds number (Gaster 1974; Saric & Nayfeh 1975). This method is not asymptotically rigorous because the $O(1)$ equation of the expansion contains the $O(1)$, $O(Re^{-1/6})$, $O(Re^{-1/3})$ and $O(Re^{-1/2}\ln Re)$ terms, which have been proved to exist in Goldstein (1983). Similarly, the $O(Re^{-1/2})$ equation contains many asymptotic sub-terms too. The study of Bertolotti, Herbert & Spalart (1992) uses this non-rigorous asymptotic method to incorporate the non-parallel effects into a single partial differential equation known as the parabolized stability equation (PSE). In the last 15 years, the PSE formulation has been used extensively with extensions to take account of hypersonic flows, nonlinearity and chemical reactions within the boundary layer flow (see for example Langlois, Casalis & Arnal 1998; Chang 2003). One advantage of incorporating the non-parallel effects into one equation is that this method replaces the algebra of eliminating singular terms with numerical computations (Saric & Nayfeh 1975). The PSE is marched downstream from some initial condition and is computationally faster than direct numerical simulations (DNS). Previous studies using the PSE (Bertolotti *et al.* 1992; Andersson, Henningson & Hanifi 1998) have initiated the code using an upstream boundary condition from Orr–Sommerfeld theory or using a local solution to the PSE, without taking complete account of the interaction of the free-stream disturbance with the boundary layer (the receptivity

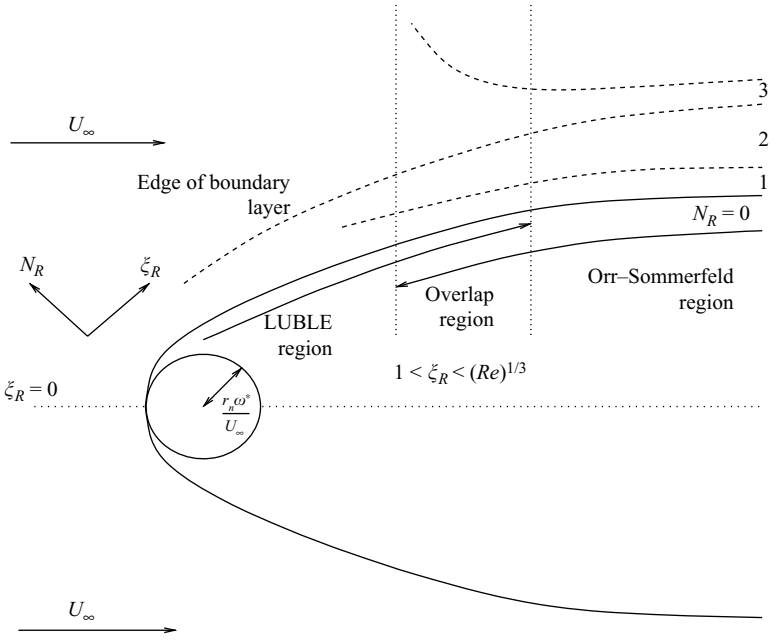

FIGURE 1. Illustration of the boundary layer structure for a general body with dimensional nose radius r_n at zero angle of attack to the mean flow. The three-deck asymptotic structure in the Orr–Sommerfeld region consists of: 1, the viscous wall layer; 2, the main inviscid layer; 3, the outer irrotational layer.

problem). Hence, these methods only give the amplitude of the unstable T-S mode up to an unknown multiplicative constant. Turner & Hammerton (2006) fix the value of this unknown constant by producing a method which combines the PSE in the Orr–Sommerfeld region with an upstream boundary condition of the Lam–Rott eigenmode from the leading edge receptivity analysis. This method allows the amplitude of the unstable T-S mode to be calculated at the lower branch neutral stability point, and allows comparison with other numerical studies (Haddad & Corke 1998). This paper extends this method to incorporate bodies with non-zero nose curvature.

For bodies with a rounded leading edge, the same asymptotic structure as for the flat plate holds along the surface of the body, as shown in figure 1. The LUBLE region is valid when the streamwise variable $\xi_R = \omega^* \xi^* / U_\infty = O(1)$, where U_∞ is the mean flow velocity and ω^* is the dimensional frequency of the free-stream disturbance. The Orr–Sommerfeld region is valid when $\xi_R = O(Re^{1/3})$, where $Re = U_\infty^2/(\omega^* \nu)$ is the Reynolds number based on the acoustic wavelength U_∞/ω^* (Goldstein 1983; Nichols 2001; Turner 2005). The asymptotic Lam–Rott eigenmodes for a flat plate have been generalized for a parabolic body by Hammerton & Kerschen (1996), who also calculate the free-stream-dependent receptivity coefficient as a function of the nose radius. This analysis has been generalized further by Nichols (2001) to bodies which have an inviscid free-stream velocity which tends to unity far downstream. Nichols also calculates the receptivity coefficient for the Rankine body as a function of the nose radius.

Numerical investigations of finite thickness bodies have been carried out mainly via DNS methods (Reed 1994). Fuciarelli, Reed & Lyttle (1998) discuss such DNS results for a flat plate with an elliptical leading edge, while the alternative approach of Corke and co-workers linearizes about the basic flow, which then decouples the steady

and unsteady flow fields that can then be solved separately. Haddad & Corke (1998) consider parabolic bodies at a zero angle of attack to the mean flow, while Erturk & Corke (2001) and Haddad, Erturk & Corke (2005) extend this to consider parabolic bodies at a non-zero angle of attack. Wanderley & Corke (2001) consider bodies with an elliptical leading edge in order to compare with the results of Fuciarelli *et al.* (1998) and the experiments of Saric & White (1998). A purely asymptotic theory for these cases is not currently available due to the algebraic complexity of the analysis, and so the numerical and experimental investigations described above cannot be compared to asymptotic theory. However, the numerical/asymptotic theory for general bodies presented in this paper will allow for direct comparisons in future studies.

The structure of this paper is as follows. Section 2 formulates the PSE for bodies with non-zero curvature, and also reviews the work of Nichols (2001) to give the general form of the leading edge asymptotic eigenmodes, which can then be used as the upstream boundary condition for the PSE. Positions of neutral stability and the amplitude of the unstable T-S modes at these points are presented in § 3 for both the parabolic body and the Rankine body. Some comments and concluding remarks are given in § 4.

2. Formulation

2.1. *Formulation of the parabolized stability equation*

In this section, we derive the parabolized stability equation (PSE) valid within the boundary layer on a two-dimensional body with a rounded leading edge. We use the coordinate system (x^*, y^*) where the dimensional coordinates x^* and y^* are measured along the body and normal to the body, respectively. Introducing dimensionless quantities based on the velocity scale U_∞ and the fixed length scale $\delta_0 = (\nu x_0^*/U_\infty)^{1/2}$, the vorticity equation can be written in terms of the stream function Ψ as

$$\left(\frac{\partial}{\partial t} - \frac{1}{R_0}\nabla^2 + \frac{\partial \Psi}{\partial y}\frac{\partial}{\partial x} - \frac{\partial \Psi}{\partial x}\frac{\partial}{\partial y}\right)\nabla^2 \Psi = 0, \tag{2.1}$$

where

$$R_0 = \frac{U_\infty \delta_0}{\nu}. \tag{2.2}$$

Here ν is the kinematic viscosity, x_0^* is the dimensional distance along the body at which the PSE analysis is started and R_0 is the Reynolds number based upon the length scale δ_0. The Reynolds number R_0 is assumed to be large so that the flow field is inviscid and irrotational everywhere, except in the vicinity of the surface of the body. The corresponding non-dimensional position that we start our analysis is $x_0 = R_0$.

The stream function is split into a steady base-flow part $\Psi_B(x, y)$ and a time-dependent disturbance part $\psi(x, y, t) \ll \Psi_B(x, y)$, and we assume that at the edge of the boundary layer, the mean flow has a slip velocity $U_f(x)$ parallel to the surface of the body. The equation for the disturbance quantity ψ is obtained by substituting $\Psi = \Psi_B + \psi$ into (2.1) and subtracting off the equation satisfied by the mean flow (Bertolotti *et al.* 1992). The resulting equation for ψ holds at leading order for the disturbance as long as the curvature of the body is assumed to be small away from the vicinity of the leading edge (Rosenhead 1963; Turner 2005). To make a comparison with the analysis in the leading edge region, formulated in § 2.2, we change our coordinate system to

$$\xi = \int_0^x U_f(x')\,\mathrm{d}x', \qquad N = R_0^{1/2} U_f(\xi)(2\xi)^{-1/2} y, \tag{2.3}$$

which remain in the streamwise and normal directions to the body, respectively (Nichols 2001; Turner 2005).

We seek a solution for the disturbance stream function $\psi(\xi, N, t)$ in the form of a spatially evolving two-dimensional wave with constant frequency ω, local streamwise wavenumber $\alpha(\xi)$ and a complex mode shape $\phi(\xi, N)$ of the form

$$\psi(\xi, N, t) = \phi(\xi, N)\exp(\mathrm{i}(\theta(\xi) - \omega t)) + \text{complex conjugate}, \tag{2.4}$$

where

$$\frac{\mathrm{d}\theta}{\mathrm{d}\xi} = \alpha(\xi).$$

The amplitude of the disturbance is assumed to be sufficiently small ($|\psi| \ll 1$) so that the nonlinear terms can be neglected. This condition suffices for the calculations in this study because we are interested only in calculating the amplitude of the unstable T-S mode up to the lower branch neutral stability point, and nonlinear effects only become significant downstream of this point if the initial disturbance amplitude is above some threshold. It is possible to calculate amplitudes up to the upper branch neutral stability point, but the nonlinear form of the PSE, which is discussed in Bertolotti *et al.* (1992), should also be considered. The main assumption in the formulation of the PSE is that the streamwise variation of α and ϕ is sufficiently small (Bertolotti *et al.* 1992; Turner & Hammerton 2006), that is $\partial^2\alpha/\partial\xi^2$, $\partial^2\phi/\partial\xi^2$ and the product of first derivatives $\partial\alpha/\partial\xi$ and $\partial\phi/\partial\xi$ are $O(R_0^{-2})$, and hence negligible if we retain only terms of $O(R_0^{-1})$ in our analysis. This assumption has been seen to hold in numerical computations (Morkovin 1985), and we have checked that these conditions hold for the values of R_0 considered in this paper.

Using these assumptions and retaining terms of $O(R_0^{-1})$ leads to the derivation of the linear PSE, which in operator form is

$$(L_0 + L_1 + L_2)\,\phi + M_1\frac{\partial\phi}{\partial\xi} + \frac{\mathrm{d}\alpha}{\mathrm{d}\xi}M_2\phi = 0, \tag{2.5}$$

where

$$L_0 = -\frac{1}{R_0}\left(\frac{R_0 D^2}{2\xi} - \alpha^2\right)^2 + \left(\frac{\mathrm{i}\alpha}{U_f}\frac{\partial\Psi_B}{\partial y} - \frac{\mathrm{i}\omega}{U_f^2}\right)\left(\frac{R_0 D^2}{2\xi} - \alpha^2\right) - \frac{\mathrm{i}\alpha}{U_f^3}\frac{\partial^3\Psi_B}{\partial y^3}, \tag{2.6}$$

$$L_1 = \frac{R_0^{1/2}}{(2\xi)^{1/2}U_f^3}\frac{\partial^3\Psi_B}{\partial x\partial y^2}D - \frac{R_0^{1/2}}{(2\xi)^{1/2}U_f}\frac{\partial\Psi_B}{\partial x}\left(\frac{R_0 D^3}{2\xi} - \alpha^2 D\right), \tag{2.7}$$

$$L_2 = \left(\frac{U_f'}{U_f} - \frac{1}{2\xi}\right)N\left(\frac{1}{U_f}\frac{\partial\Psi_B}{\partial y}\left(\frac{R_0 D^3}{2\xi} - 3\alpha^2 D\right) + \frac{2\omega\alpha}{U_f^2}D - \frac{1}{U_f^3}\frac{\partial^3\Psi_B}{\partial x\partial y^2}D\right)$$
$$+ \frac{2R_0}{U_f}\frac{\partial\Psi_B}{\partial y}\left(\frac{U_f'}{2\xi U_f} - \frac{1}{4\xi^2}\right)D^2 + \frac{\omega\alpha U_f'}{U_f^3} - \frac{3U_f'\alpha^2}{U_f^2}\frac{\partial\Psi_B}{\partial y}, \tag{2.8}$$

$$M_1 = \frac{1}{U_f}\frac{\partial\Psi_B}{\partial y}\left(\frac{R_0 D^2}{2\xi} - 3\alpha^2\right) + \frac{2\omega\alpha}{U_f^2} - \frac{1}{U_f^3}\frac{\partial^3\Psi_B}{\partial x\partial y^2}, \tag{2.9}$$

$$M_2 = \frac{\omega}{U_f^2} - \frac{3\alpha}{U_f}\frac{\partial\Psi_B}{\partial y}, \tag{2.10}$$

and $D \equiv \partial/\partial N$. For a semi-infinite flat plate, $U_f = 1$ and the system of equations (2.5–2.10) is equivalent to the governing equations in Turner & Hammerton (2006).

In (2.4) there is ambiguity in the choice of functions $\alpha(\xi)$ and $\phi(\xi, N)$. To resolve this we introduce a normalization condition on ϕ which restricts the rapid variation in the ξ direction. We define this normalization condition as

$$\int_0^\infty \phi_\xi \phi^\dagger \, \mathrm{d}N = 0, \tag{2.11}$$

where † denotes the complex conjugate. This normalization condition is equivalent to

$$\int_0^\infty |\psi|^2 \, \mathrm{d}N = C \exp(-2\mathrm{Im}(\theta(\xi))),$$

which shows that the majority of the streamwise variation with ξ is now in the wavenumber $\alpha(\xi)$. This normalization condition minimizes the streamwise change $\partial\phi/\partial\xi$ in a weighted sense over the N domain, which also keeps $\partial\phi/\partial\xi$ small in accordance with our initial assumption. Other normalization conditions could be implemented (Herbert 1993; Andersson *et al.* 1998); however, we find this one to be most desirable because it gives results which are in excellent agreement with those for a boundary layer on a flat plate (Turner & Hammerton 2006). Although the formulation does not prove that a solution satisfying (2.11) exists, the agreement of the PSE results with those of Goldstein (1983) for a flat plate justifies this choice (Turner 2005; Turner & Hammerton 2006).

Equations (2.5) and (2.11) are solved numerically via a spectral collocation technique using Chebyshev polynomials. This method is equivalent to that described in Turner & Hammerton (2006) and Bertolotti *et al.* (1992), and so the reader is directed to these for more details.

In this study, we are interested only in the propagation of the eigenmodes from the leading edge region through the Orr–Sommerfeld region, and hence we solve (2.5) with homogeneous boundary conditions and an upstream boundary condition stipulated by

$$\phi(\xi_0, N) = \hat{F}(N), \qquad \alpha(\xi_0) = \alpha_0, \tag{2.12}$$

where ξ_0 is the dimensionless starting position for the analysis along the surface of the body. These conditions depend upon the form of the boundary layer at ξ_0 and the interaction of the free-stream disturbance with the boundary layer upstream of this point.

2.2. *Leading edge receptivity analysis*

Near to the leading edge of the body, the PSE is no longer valid because the boundary layer grows rapidly in this region and the assumption that $\alpha_{\xi\xi}$, $\phi_{\xi\xi}$ and $\alpha_\xi \phi_\xi$ are small breaks down. In this region we have a different balance of terms at leading order as opposed to § 2.1. The solution for the mode shape in this region has a three-deck structure: the bottom deck is a Stokes layer solution where viscosity is important; the solution in this deck satisfies the no-slip condition at the wall. An outer inviscid region occurs outside the boundary layer and the solution here tends to zero for large N. Between these two layers is the main inviscid layer within the boundary layer where the solution must match to the other two solutions in the appropriate limits.

In the leading edge receptivity region the slip velocity at the edge of the boundary layer U_s is assumed to have a steady part and a linear perturbation due to the harmonic external disturbance,

$$U_s(x_R, t) = U_f(x_R) + \hat{\epsilon} U_d(x_R) \mathrm{e}^{-\mathrm{i}t}. \tag{2.13}$$

Here $\hat{\epsilon} \ll 1$, x_R is the streamwise coordinate non-dimensionalized by the acoustic length scale U_∞/ω^* and ω^* is the dimensional frequency of the small-amplitude perturbation. We define $Re = \epsilon^{-6} = U_\infty^2/(\nu\omega^*)$ to be the Reynolds number based on this acoustic length scale, which is assumed to be large, so the parameter ϵ is small.

We seek a solution to the non-dimensional form of (2.1), derived in the receptivity variables (x_R, y_R), of

$$\Psi_R = \frac{(2\xi_R)^{1/2}}{Re^{1/2}}\left(\phi_1(\xi_R, N_R) + \phi_2(\xi_R, N_R)\mathrm{e}^{-\mathrm{i}t}\right),$$

where

$$\xi_R = \int_0^{x_R} U_f(x')\,\mathrm{d}x' \quad \text{and} \quad N_R = \frac{U_f(\xi_R)Re^{1/2}}{(2\xi_R)^{1/2}}y_R. \tag{2.14}$$

The subscript R denotes that we are in the receptivity region of the body. Neglecting higher order terms in inverse powers of Re and equating powers of $\hat{\epsilon}$ we find that the steady equation for $\phi_1(\xi_R, N_R)$ is

$$\phi_{1N_RN_RN_R} + \phi_1\phi_{1N_RN_R} = \beta(\xi_R)\left(\phi_{1N_R}^2 - 1\right) + 2\xi_R\left(\phi_{1N_R}\phi_{1N_R\xi_R} - \phi_{1N_RN_R}\phi_{1\xi_R}\right), \tag{2.15}$$

where $\beta(\xi_R) = 2\xi_R U_f^{-1}\,\mathrm{d}U_f/\mathrm{d}\xi_R$ is the mean pressure gradient along the surface of the body. Equation (2.15) is solved with the boundary conditions $\phi_1 = \phi_{1N_R} = 0$ on $N_R = 0$ and $\phi_{1N_R} \to 1$ as $N_R \to \infty$. The unsteady flow component $\phi_2(\xi_R, N_R)$ satisfies

$$\begin{aligned}\phi_{2N_RN_RN_R} + \phi_{2N_RN_R}\left(\phi_1 + 2\xi_R\phi_{1\xi_R}\right) + \phi_{2N_R}\left(\mathrm{i}\Omega(\xi_R) - 2\beta(\xi_R)\phi_{1N_R} - 2\xi_R\phi_{1N_R\xi_R}\right)\\ + \phi_2\phi_{1N_RN_R} + 2\xi_R\left(\phi_{1N_RN_R}\phi_{2\xi_R} - \phi_{1N_R}\phi_{2N_R\xi_R}\right) = h(\xi_R),\end{aligned} \tag{2.16}$$

where $\Omega(\xi_R) = 2\xi_R/U_f^2$ and the boundary conditions are $\phi_2 = \phi_{2N_R} = 0$ on $N_R = 0$ and $\phi_{2N_R} \to U_d(\xi_R)/U_f(\xi_R)$ as $N_R \to \infty$. The function $h(\xi_R)$ is determined by the unsteady forcing of the boundary layer by the free-stream disturbance. Equation (2.16) is known as the linearized unsteady boundary layer equation (LUBLE).

We assume that far downstream ($x_R \longrightarrow \infty$), the steady form of the slip velocity $U_f(x_R)$ acts parallel and symmetric to the surface of the body. Thus, the asymptotic form of $U_f(x_R)$ in this limit is

$$U_f(x_R) = 1 + \frac{\gamma_1}{x_R} + \frac{\gamma_2}{x_R^2} + O\left(x_R^{-3}\right), \tag{2.17}$$

or using (2.14)

$$U_f(\xi_R) = 1 + \frac{\gamma_1}{\xi_R} + \frac{\gamma_1^2\ln(\xi_R)}{\xi_R^2} + \frac{\gamma_2}{\xi_R^2} + O\left(\xi_R^{-3}\ln^2(\xi_R)\right), \tag{2.18}$$

where γ_1 and γ_2 are real constants.

In this limit the steady solution for $\phi_1(\xi_R, N_R)$ can be determined as

$$\phi_1(\xi_R, N_R) = f - 1.2023\gamma_1(N_Rf' - f)\frac{\ln(\xi_R)}{\xi_R} + \frac{D(N_Rf' - f) + \gamma_1 E(N_R)}{\xi_R} + O(\xi_R^{-1.887}), \tag{2.19}$$

where $f(N_R)$ is the Blasius function which satisfies

$$f''' + ff'' = 0, \qquad f(0) = f'(0) = 0, \qquad f' \longrightarrow 1 \quad \text{as} \quad N_R \longrightarrow \infty,$$

and the prime denotes $\mathrm{d}/\mathrm{d}N_R$. The constant D in (2.19) is calculated numerically and depends upon the curvature of the body (Hammerton & Kerschen 1996; Nichols

2001; Turner 2005). The function $E(N_R)$ is also calculated numerically by solving the differential equation

$$E''' + fE'' + 2f'E' - f'E = -2(f'-1) - 2.4046ff'',$$

with $E = E' = E'' = 0$ at $N_R = 0$. The correction terms to (2.19) correspond to non-integer eigenvalues of (2.15) (Libby & Fox 1963).

In the limit of large ξ_R the solution for ϕ_2 consists of a Stokes solution, which depends on the form of the unsteady disturbance $U_d(\xi_R)$, and a sum of asymptotic eigenmodes which satisfy (2.16) with $h(\xi_R) = 0$ and with homogeneous boundary conditions (Lam & Rott 1960, 1993; Brown & Stewartson 1973). The precise relationship between these two sets of eigenmodes is unclear (Hammerton 1999); however, the Lam–Rott eigenmodes are important in receptivity as they exhibit the wavelength shortening needed to convert the long-wavelength free-stream disturbances to short-wavelength disturbances in the boundary layer. Nichols (2001) calculates the form of these Lam–Rott eigenmodes for a general body with an asymptotic steady-slip velocity as in (2.17). The jth eigenmode takes the form

$$\psi_j^{LR}(\xi_R, N_R) = (2\xi_R)^{1/2}\phi_2(\xi_R, N_R) = C_j \xi_R^{\tau_j} g_0(\xi_R, N_R) \mathrm{e}^{T_j(\xi_R)}, \tag{2.20}$$

where C_j is an arbitrary constant dependent on the curvature of the body known as the receptivity coefficient. The constants τ_j are expressed in terms of ρ_j and γ_1, where ρ_j is the jth root of the equation $\mathrm{Ai}'(-\rho_j) = 0$ and Ai′ is the derivative of the Airy function of the first kind. The function $T_j(\xi_R)$ is given by

$$T_j(\xi_R) = -\frac{\mathrm{e}^{-\mathrm{i}\pi/4}(2\xi_R)^{3/2}}{U_0'\rho_j^{3/2}}\left(\frac{1}{3} + 1.2023\gamma_1\frac{\ln(\xi_R)}{\xi_R} + (-5.4046\gamma_1 - D)\frac{1}{\xi_R}\right) + O\left(\xi_R^{-0.387}\right),$$

where $U_0' = f''(0) = 0.4696$. In this study, we are interested only in the propagation of the first of these eigenmodes as it is this mode which matches onto the spatially growing T-S mode in the Orr–Sommerfeld region (Goldstein 1983); hence $\rho_1 = 1.0188$ and $\tau_1 = -0.6921 - 7.9508\gamma_1\mathrm{i}$ (Nichols 2001; Turner 2005). The function $g_0(\xi_R, N_R)$ can be represented in the leading edge region as a composite of the three-deck solutions (Turner 2005; Turner & Hammerton 2006) and can be written as

$$g_0(\xi_R, N_R) = \xi_R^{\tau_1}\left((2\xi_R)^{1/2}f'(N_R) + U_0'\frac{\int_0^M (M-\widetilde{M})\mathrm{Ai}(\tilde{z})\mathrm{d}\widetilde{M}}{\int_0^\infty \mathrm{Ai}(\tilde{z})\mathrm{d}\widetilde{M}} - U_0'(2\xi_R)^{1/2}N_R\right) \times \exp\left(-\frac{\epsilon^3\sqrt{2}(1+\mathrm{i})\xi_R N_R}{U_0'\hat{\gamma}(\xi_R)\rho_1^{3/2}}\right), \tag{2.21}$$

where

$$M = (2\xi_R)^{1/2}\left(1 - \frac{\gamma_1}{\xi_R}\right)N,$$

$$\tilde{z} = -\rho_1 + \rho_1^{-1/2}\mathrm{e}^{\mathrm{i}\pi/4}\widetilde{M},$$

$$\hat{\gamma} = 1 - 1.2023\gamma_1\frac{\ln(\xi_R)}{\xi_R} + (D + 3\gamma_1)\frac{1}{\xi_R} + O\left(\xi_R^{-1.887}\right).$$

Equation (2.20) with $g_0(\xi_R, N_R)$ given by (2.21) is now used as the initial condition for the PSE calculations where the PSE and the receptivity variables are related to

one another by

$$\xi_R = \frac{R_0}{Re}\xi \quad \text{and} \quad N_R = N.$$

Hence, we start our analysis for the PSE calculation at the scaled streamwise receptivity variable $\tilde{\xi}_1 = \tilde{\xi}_1^{(0)}$ where

$$\xi_0 = R_0 = \epsilon^{-4} U_0' \left(\frac{\tilde{\xi}_1^{(0)}}{2}\right)^{1/2}, \quad \omega = \frac{R_0}{Re},$$

and $\epsilon = Re^{-1/6}$. The variable $\tilde{\xi}_1 = 2\epsilon^2 \xi_R / U_0'^2$ is introduced to make comparisons with the works of Goldstein (1983) and Turner & Hammerton (2006) easier. Thus, from (2.12) and (2.20) the initial wavenumber is given by

$$\alpha(\xi_0) = \frac{\mathrm{i}\epsilon^6 R_0 \mathrm{e}^{-\mathrm{i}\pi/4} \left(\tilde{\xi}_1^{(0)}\right)^{1/2}}{\rho_1^{3/2}} \left(1 + 1.2023\gamma_1 \frac{\ln(\xi_0)}{\xi_0} - (D + 3\gamma_1)\frac{1}{\xi_0}\right), \tag{2.22}$$

and the form of the base flow is given by

$$\Psi_B = \frac{(2\xi)^{1/2}}{R_0^{1/2}} \left(f - 1.2023\gamma_1 \frac{Re}{R_0}(Nf_N - f)\frac{\ln(R_0\xi/Re)}{\xi} + \frac{Re}{R_0}\frac{D(Nf_N - f) + \gamma_1 E(N)}{\xi}\right) + O(\xi^{-1.387}).$$

Alternative forms for the initial condition to the PSE include using the most unstable eigenmode of the Orr–Sommerfeld equation or the local PSE at $\xi = \xi_0$. However, the advantage of the receptivity condition is that it contains all the information required to give the amplitude of the unstable T-S mode as it enters the Orr–Sommerfeld region, and hence we have the complete T-S mode amplitude at the lower branch point. This is discussed in more detail in Turner & Hammerton (2006) for the case of a flat plate.

3. Results

In this section we present results giving the position of the lower branch neutral stability point and the amplitude of the unstable T-S mode at this point for bodies with a slip velocity which has the form given in (2.17). It is noted from (2.20) that to have the complete amplitude of the unstable T-S mode as it enters the Orr–Sommerfeld region, we need to know the value of the receptivity coefficient $|C_1|$ which varies as a function of the nose curvature of the body. Hence in this section we present results for bodies for which the value of $|C_1|$ has been calculated. Therefore, we consider a parabolic body (Hammerton & Kerschen 1996) and the Rankine body (Nichols 2001). In the remainder of this section, we use the superscripts P and R to represent the parabola and the Rankine body, respectively.

The calculation of the position of the neutral stability point can be made easier by placing all the wave amplitude information into one single growth-rate function. This is achieved by splitting the amplitude function in (2.4) in the following way:

$$\phi(\xi, N) = \phi_{max}(\xi)\bar{\phi}(\xi, N),$$

where the maximum value of $\bar{\phi}$ is 1. Thus, the stream function is given by

$$\psi = \bar{\phi}(\xi, N)\exp(\mathrm{i}\tilde{\theta}(\xi) - \omega t) + \text{complex conjugate}, \quad \text{with} \quad \frac{\mathrm{d}\tilde{\theta}}{\mathrm{d}\xi} = G(\xi),$$

where all the wave amplitude information is now contained in the growth rate $G(\xi)$, which, when written as a function of the receptivity variable ξ_R, has the form

$$G(\xi_R) = \frac{Re}{R_0}\left(\mathrm{i}\alpha + \frac{1}{\phi_{max}}\frac{\partial \phi_{max}}{\partial \xi}\right). \tag{3.1}$$

The lower branch neutral stability point can now be defined as the position where $\mathrm{Im}(G) = 0$. Although $G(\xi_R)$ is defined as a function of the streamwise variable ξ_R, we usually display our results in terms of the scaled receptivity variable $\tilde{\xi}_1 = 2\epsilon^2 \xi_R / U_0'^2$ as this makes comparisons with the flat-plate analysis of Goldstein (1983) and Turner & Hammerton (2006) easier.

In this study, we are interested in calculating the amplitude of the unstable T-S mode ψ_1, from (2.20), which is achieved by integrating the growth rate $G(\xi_R)$ from a position within the matching region between the leading edge and the Orr–Sommerfeld regions, ξ_R^{LE}, to the lower branch (branch I) neutral stability point ξ_R^I. The value of ξ_R^{LE} can take any value in the region close the leading edge where the downstream amplitude is independent of the value of ξ_R^{LE}. This region has been shown to exist for a flat plate by Turner & Hammerton (2006). Thus, the amplitude of ψ_1 at the branch I neutral stability point can be written as

$$\left|\psi_1^I\right| = \left|C_1 \psi_1^{LR}\left(\xi_R^{LE}\right) \exp\left(\int_{\xi_R^{LE}}^{\xi_R^I} G(x)\,\mathrm{d}x\right)\right|. \tag{3.2}$$

Throughout this study, we shall refer to $|\psi_1^I|$ as the T-S mode amplitude at the lower branch neutral stability point, and $|C_1^{-1}\psi_1^I|$ as the eigenmode amplitude at this point.

An important factor needed in order to use this PSE method is the existence of a matching region between the leading edge asymptotic result and the result in the Orr–Sommerfeld region. This was shown to exist for a flat plate in Turner & Hammerton (2006) for sufficiently small ϵ and figure 2 shows that the same is true for the parabola where $S = r_n \omega^* / U_\infty$ is the Strouhal number and corresponds to the dimensionless nose radius of the parabola. The figure shows $Re(G(\tilde{\xi}_1))$ for two nose radii and for (a) $\epsilon = 0.05$ and (b) $\epsilon = 0.1$. The leading edge solution is given by (3.1) with α replaced by (2.22) and the local PSE result is a solution of (2.5) about $\tilde{\xi}_1$ for each $\tilde{\xi}_1$. For more details on the local PSE solution, see Bertolotti *et al.* (1992) and Turner & Hammerton (2006). The local PSE is an indication of how close to the nose of the body the PSE solution can be before the PSE code fails converge to the correct growth rate because of initial transients in the solution (Turner & Hammerton 2006). Figure 2(a) shows that a clear matching region exists, and thus for small values of $\epsilon = Re^{-1/6}$ the PSE can be started back in the matching region near ξ_R^{LE}, and so the growth rate is defined over the whole domain of integration. However, for larger values of ϵ, the PSE code cannot be initiated back in the matching region as can be seen in figure 2(b). We overcome this problem by patching the growth rate back to ξ_R^{LE} using the same method as in Turner & Hammerton (2006). This method involves fixing the value of the growth rate and its derivative using both the leading edge solution and the PSE solution, and then patching the region in between by a cubic polynomial with complex coefficients. For more information on this patching method and its validity, see Turner & Hammerton (2006). Care was taken to ensure that the wave amplitude downstream was independent of the step size chosen and also not

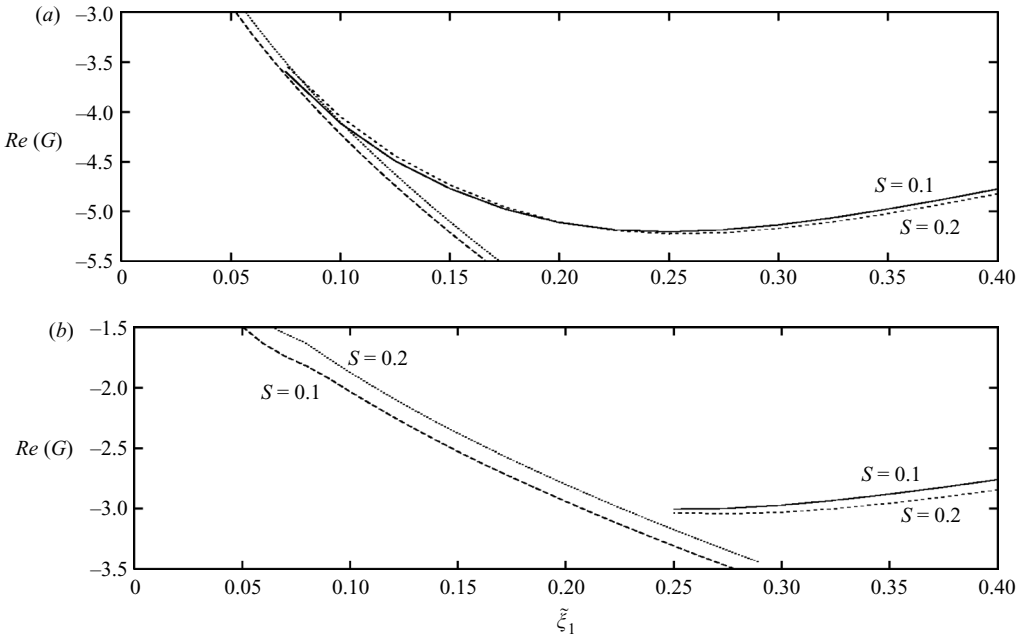

FIGURE 2. Plot of the real part of the growth rate $G(\tilde{\xi}_1)$ as a function of downstream distance $\tilde{\xi}_1 = 2\epsilon^2 \xi_R / U_0'^2$, calculated by the leading edge receptivity analysis and local PSE theory, for $S = 0.1$ and $S = 0.2$ for the cases (*a*) $\epsilon = 0.05$ and (*b*) $\epsilon = 0.1$.

sensitive to the choice of streamwise position at which the PSE solution was patched to the receptivity analysis.

The parabolic body is described in terms of the Strouhal number, while the Rankine body is described in terms of the dimensionless parameter $A = 2r_n\omega^*/3U_\infty$, which is linked to the dimensionless nose radius $3A/2$ (Turner 2005). Thus, the two bodies have the same nose radius if $S = 3A/2$. The inviscid flow around the parabolic body is calculated using slender body theory (Hammerton & Kerschen 1996), while the inviscid flow around the Rankine body is determined by complex potential theory (Nichols 2001). The forms of the slip velocity U_f at the edge of the boundary layer for these bodies are

$$U_f^P(\xi_R) = \frac{(2\xi_R)^{1/2}}{(2\xi_R + S)^{1/2}}, \tag{3.3}$$

$$U_f^R(y_c) = \left(1 + \frac{A^2}{y_c^2}\sin^2\left(\frac{y_c}{A}\right) - \frac{A}{y_c}\sin\left(\frac{2y_c}{A}\right)\right)^{1/2}, \tag{3.4}$$

where y_c is the Cartesian y-coordinate. The large ξ_R form of each slip velocity can be calculated as

$$U_f^P = 1 - \frac{S}{4\xi_R} + \frac{3S^2}{32\xi_R^2} + O\left(\xi_R^{-3}\right), \tag{3.5}$$

$$U_f^R = 1 + \frac{A}{\xi_R} + \frac{A^2\ln(\xi_R)}{\xi_R^2} + \frac{A^2}{x_R^2} + O\left(\xi_R^{-3}\ln^2(\xi_R)\right). \tag{3.6}$$

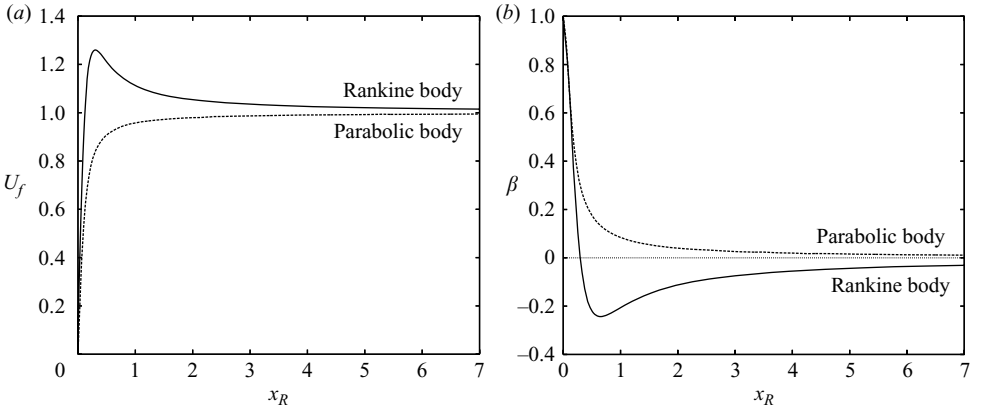

FIGURE 3. Plot of (*a*) $U_f(x_R)$ and (*b*) $\beta(x_R)$ for the Rankine body and the parabolic body with the same nose radius $S = 0.15$ ($A = 0.1$).

Thus, comparing these expressions with (2.18) we see that $\gamma_1^P = -S/4$ and $\gamma_1^R = A$. The respective values of the constant D in (2.19) can thus be calculated as

$$D^P = \frac{S}{2}\left(2.075 - 0.60115 \ln\left(\frac{S}{2}\right)\right), \tag{3.7}$$

$$D^R = A\left(-4.71125 + 1.2023 \ln(A)\right), \tag{3.8}$$

for the parabolic and Rankine bodies, respectively.

From (3.3) and (3.4), the mean pressure gradient $\beta(x_R)$ can be calculated, and figure 3 plots both (*a*) $U_f(x_R)$ and (*b*) $\beta(x_R)$ for the parabolic and Rankine bodies with the same nose radius ($A = 0.1$, $S = 0.15$). These quantities are plotted as functions of x_R because this variable is independent of the curvature of the body, whereas ξ_R is a function of A and S (see (2.14)). The parabolic body has a slip velocity which is always less than 1 and this gives a favourable (or positive) pressure gradient along the surface of the body. The Rankine body has a slip velocity which rises above 1 before asymptoting to 1 as $x_R \longrightarrow \infty$ and this gives an adverse (or negative) pressure gradient along the majority of the body's surface. The absolute value of the pressure gradient is larger on the Rankine body than on the parabolic body for $x_R \geqslant 1$, and this affects the position of the neutral stability point as we shall see later.

We now consider numerical results for three values of the Reynolds number, corresponding to $\epsilon = 0.05,\ 0.1$ and 0.2. The small value of epsilon examines the large Reynolds number asymptotic limit, and if asymptotics are developed for either of these bodies then this value of ϵ would allow for an easy comparison. The middle value of ϵ is too large for experimental data, but it is comfortably in the range of Reynolds numbers that could be used in a DNS model to verify our results. The largest value of ϵ is in the range of values that could be considered by experimentalists and DNS. This value of ϵ corresponds to a dimensionless frequency of $F = \omega^* \nu / U_\infty^2 = \epsilon^6 = 64 \times 10^{-6}$ which lies in the tail of the neutral stability curve (see Haddad & Corke 1998). This value is also at the lower edge of the values used in the DNS study of Haddad & Corke. The top of the neutral stability curve tail has values of $\epsilon \lesssim 0.25$, and so the values of ϵ considered in this paper give a good understanding of the structure behind T-S wave propagation on a body with non-zero nose radius.

Figures 4 and 5 plot the position of the lower branch neutral stability point for both the parabolic body and the Rankine body respectively for the three values of

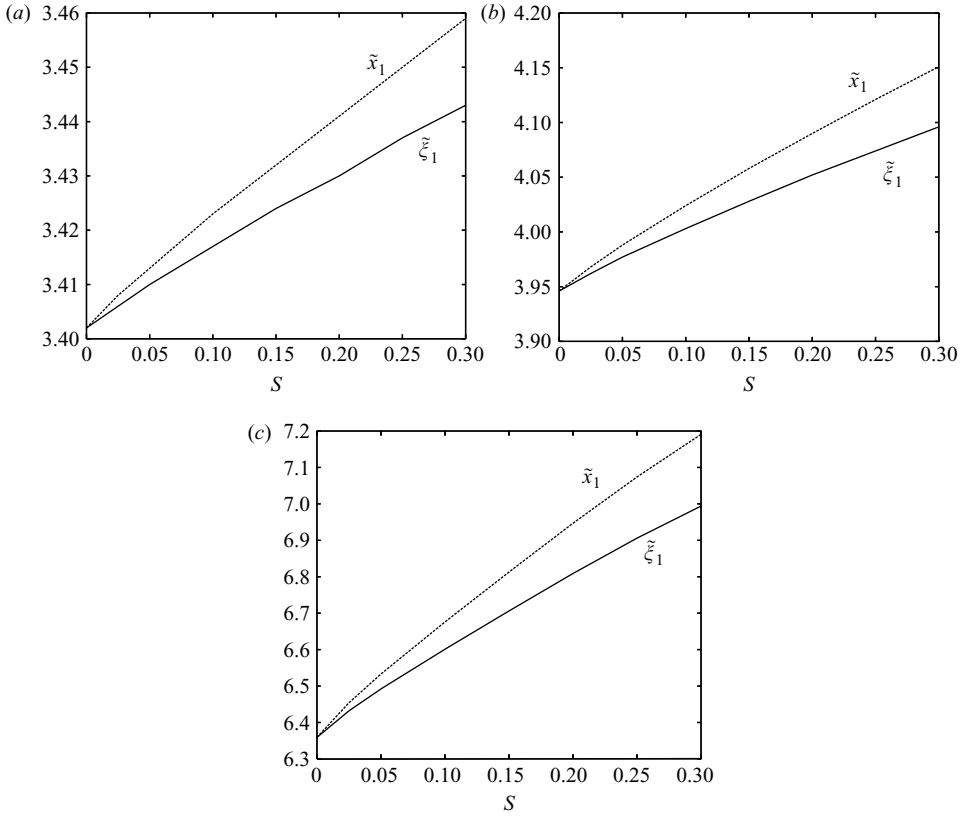

FIGURE 4. Plot of the neutral stability point on a parabolic body as a function of S for both $\tilde{\xi}_1$ and $\tilde{x}_1$ for (*a*) $\epsilon = 0.05$, (*b*) $\epsilon = 0.1$ and (*c*) $\epsilon = 0.2$.

$\epsilon = 0.05$, 0.1 and 0.2. In each figure, we plot the neutral stability point as both a function of $\tilde{\xi}_1 = 2\epsilon^2 \xi_R / U_0'^2$ and $\tilde{x}_1 = 2\epsilon^2 x_R / U_0'^2$, as the latter is independent of the nose curvature. The small bumps occurring in the solution are due to numerical error, and appear to diminish as ϵ is increased because the scale of the figures increases as ϵ is increased. Figure 4 shows that the favourable pressure gradient along the surface of the parabolic body gives a lower branch neutral stability point which is further downstream than the corresponding flat-plate value ($S = 0$). For the larger value of $\epsilon = 0.2$ in figure 4(*c*), the relative position of the neutral stability point moves even further downstream. The adverse pressure gradient on the Rankine body on the other hand gives a neutral stability point positioned nearer to the nose of the body as the nose radius ($3A/2$) is increased. This is shown in figure 5. Again, as ϵ is increased from 0.05 in figure 5(*a*) to 0.2 in figure 5(*c*), the relative position of the neutral point moves further downstream when compared to the flat-plate value.

A comparison of the deviation away from the flat-plate neutral stability point $|\tilde{x}_1 - \tilde{x}_1^{FP}|$ for both bodies is given in figure 6. For the values of ϵ considered here, $\tilde{x}_1^{FP} = 3.402$, 3.946 and 6.359 for $\epsilon = 0.05$, 0.1 and 0.2, respectively. Due to the magnitude of the adverse pressure gradient on the Rankine body being larger than that of the parabolic body at the same streamwise position (see figure 3), we note that the neutral stability point on the Rankine body is displaced further from the

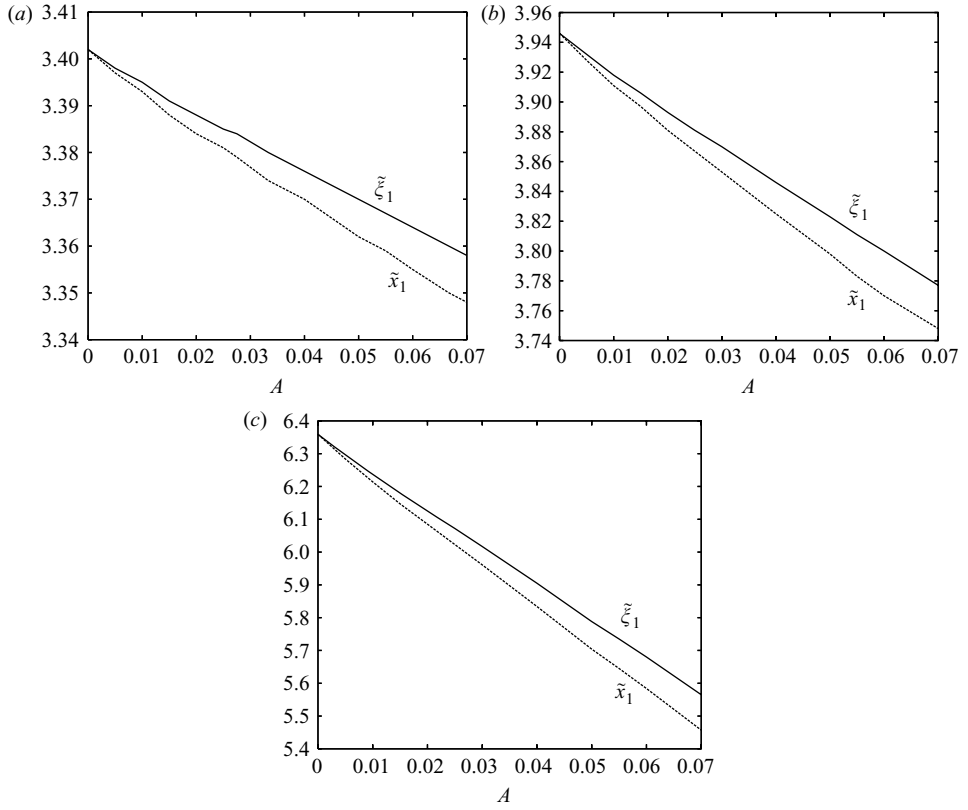

FIGURE 5. Plot of the neutral stability point for the Rankine body as a function of A for both $\tilde{\xi}_1$ and $\tilde{x}_1$ for (*a*) $\epsilon = 0.05$, (*b*) $\epsilon = 0.1$ and (*c*) $\epsilon = 0.2$.

flat-plate value than the parabolic body for the same nose radius. As ϵ increases, the difference in displacement from the flat-plate value increases between the two bodies.

Having considered the position of the point of neutral stability, we now consider the wave amplitude at this point as this affects the location of any transition point downstream of the lower branch point. In figures 7 and 8, we plot log plots of the amplitude of the unstable T-S mode $|\psi_1^I|$ defined in (2.20) at the lower branch (branch I) neutral stability point along with the corresponding amplitude of the eigenmode $|C_1^{-1}\psi_1^I|$. The results for small ϵ have unphysically small amplitudes; however, we merely use these small ϵ values to study the underlying mathematical structure of the solution, rather than for comparison with DNS or experiments. These small amplitudes suggest that the leading edge receptivity may be dominated by another receptivity mechanism, such as acoustic wave interaction with surface roughness elements, but this requires further analysis. For the parabolic body in figure 7, we see that the amplitude of the eigenmode at lower branch $|C_1^{-1}\psi_1^I|$ decreases as S increases for all the values of ϵ considered. When we include the effect of the receptivity coefficient C_1, the overall amplitude of the T-S mode $|\psi_1^I|$ decays even faster. However, Hammerton & Kerschen (1996) found that the Strouhal number $S = 0.025$ gives a receptivity coefficient $|C_1|$ that is larger than the flat-plate value. For the smallest value of ϵ considered here, $\epsilon = 0.05$, the decay rate of the eigenmode is large enough so that the T-S mode amplitude still decreases from the flat-plate value

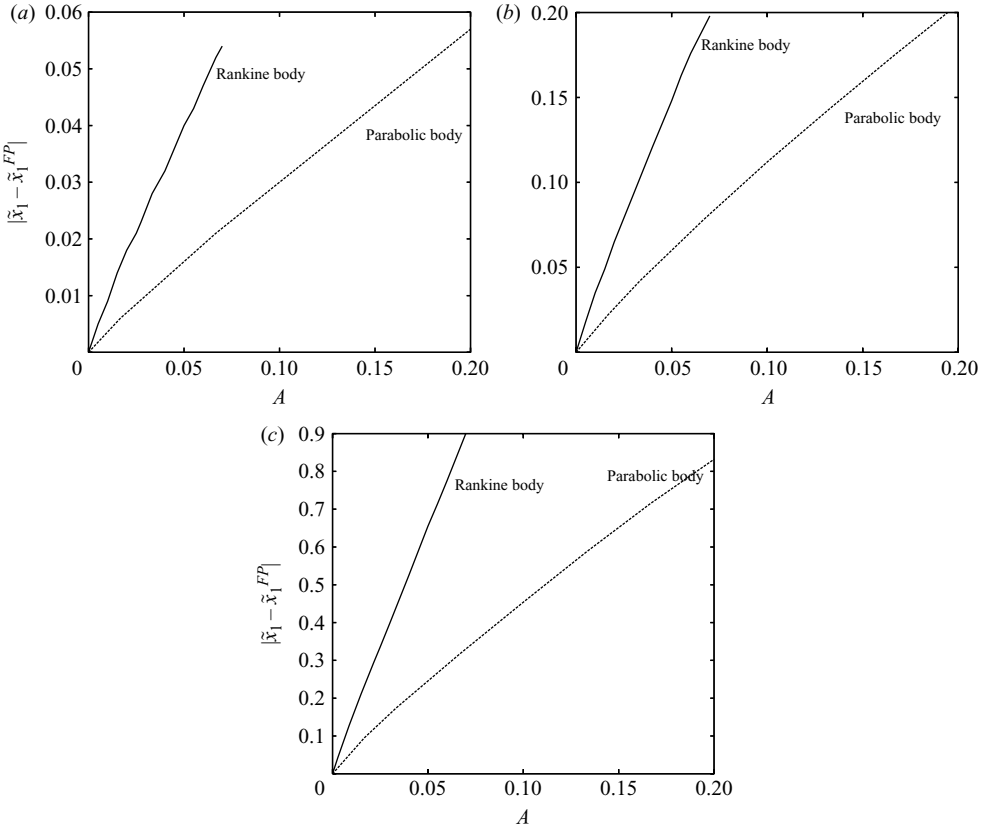

FIGURE 6. Plot of $|\tilde{x}_1 - \tilde{x}_1^{FP}|$ for the parabolic body and the Rankine body as a function of A ($S = 3A/2$) for (*a*) $\epsilon = 0.05$, (*b*) $\epsilon = 0.1$ and (*c*) $\epsilon = 0.2$.

for $S = 0.025$, but for sufficiently small ϵ it is likely that there will be a range of S for which the T-S mode amplitude at lower branch is larger than for the flat-plate case. This remains an area of future research as the numerical study of Haddad & Corke (1998) does not show an increase in T-S mode amplitude above the flat-plate value either, but it is not clear if they were in the correct parameter range to see this behaviour. However, for the reasons discussed earlier, any such increase is unlikely to have any physical significance.

For the values of ϵ considered in this study, the amplitude of the T-S mode for the Rankine body has a more interesting structure than for the parabolic body, because there is conflict between the eigenmode amplitude which increases as A increases, and the receptivity coefficient which decreases as A increases. The actual receptivity coefficient $|C_1|$ for the Rankine body tends to zero much faster than for the parabolic body because of the adverse pressure gradient, and so this gives a much smaller range of nose radii with non-zero receptivity coefficient available to us to study (Nichols 2001). The resulting T-S mode and eigenmode amplitudes for the Rankine body can be seen in the log plot in figure 8. The amplitude of the eigenmode appears to have almost an exponential growth in A, but due to the variation of the receptivity coefficient with A, the amplitude of the T-S mode has a double-maximum appearance as a function of A. For the $\epsilon = 0.05$ case in figure 8(*a*), this double maximum is very clear, with maxima around $A = 0.015$ and $A = 0.055$, and the second maximum

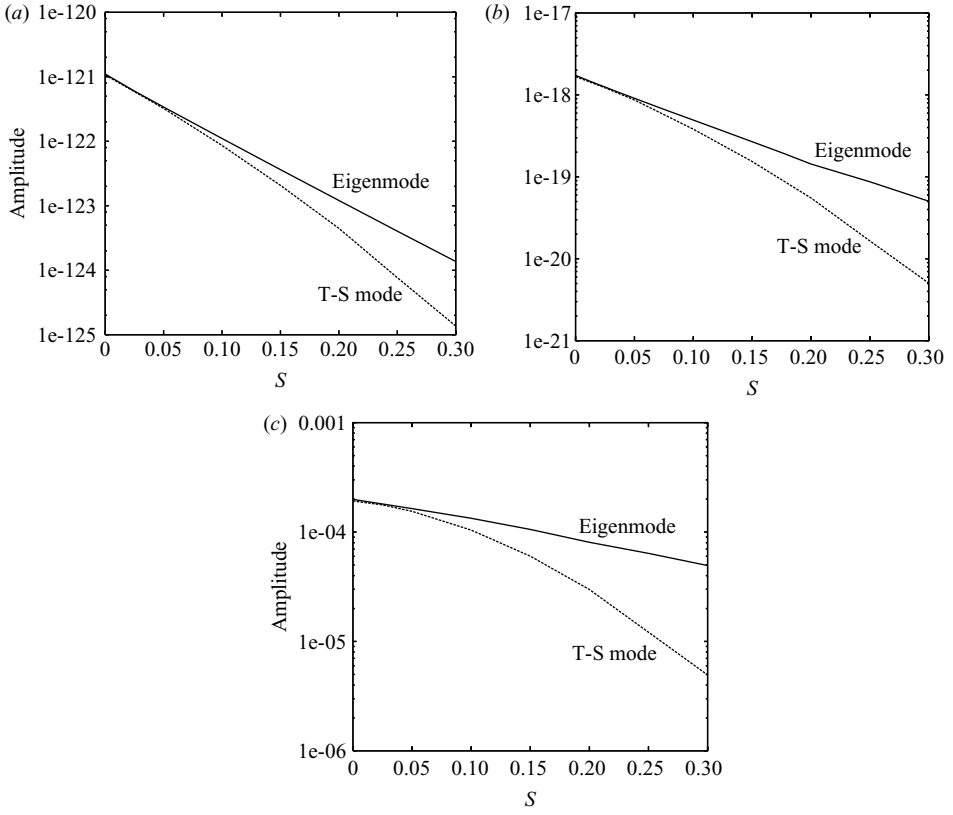

FIGURE 7. Amplitude plot on a log scale for the eigenmode $|C_1^{-1}\psi_1^I|$ and the unstable T-S mode $|\psi_1^I|$ for a parabolic body at the lower branch neutral stability point as a function of S for (a) $\epsilon = 0.05$, (b) $\epsilon = 0.1$ and (c) $\epsilon = 0.2$.

is almost a factor of 10 larger than the first. The case $\epsilon = 0.1$ in figure 8(b) has a slightly different appearance, because the rate of increase of the eigenmode amplitude is smaller than the $\epsilon = 0.05$ case, while the values of the receptivity coefficients remain unchanged. Hence, in this case the first maximum of the T-S mode amplitude is closer to $A = 0$, and in fact on the log scale the amplitude appears almost constant at the flat-plate value $A = 0$ up to $A = 0.015$. There is still another maximum around $A = 0.05$, but the relative size of this maximum compared to the first one is much smaller than for the $\epsilon = 0.05$ case, and is only a factor of 1.8 times larger. Figure 8(c) shows the same plot again except with $\epsilon = 0.2$. For this value of ϵ, the T-S mode amplitude is seen to decay away from $A = 0$, and the second maximum which occurs around $A = 0.04$ has a lower magnitude than the one at $A = 0$. Therefore as ϵ increases, the growth of the eigenmode with respect to A decreases, and hence for the $\epsilon = 0.05$ case, we find the two maxima are larger than the flat-plate value, whereas for $\epsilon = 0.2$, the first maximum now corresponds to the flat-plate value, and the second maximum has a value lower than the flat-plate value. Thus, we expect that experimental studies on a Rankine body will not produce a maximum value greater than the flat-plate value for any nose radius, because typical Reynolds numbers in experiments give $\epsilon > 0.2$. However, the experiment should still give a second increase in the T-S mode amplitude at a larger nose radii.

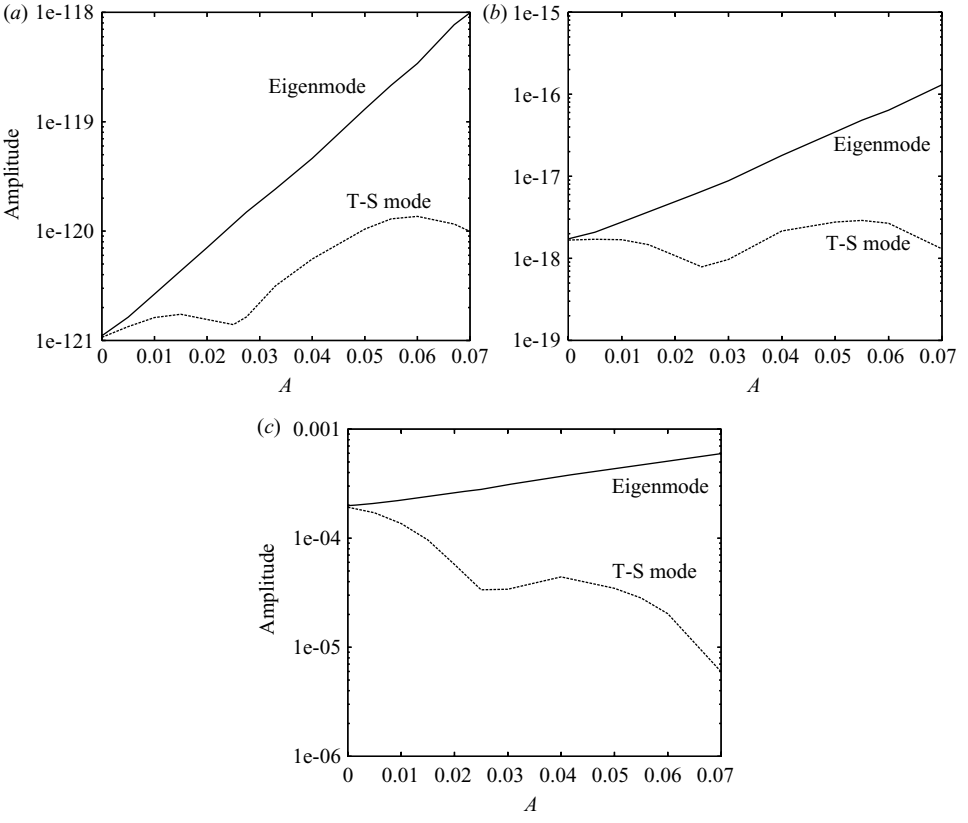

FIGURE 8. Amplitude plot on a log scale for the eigenmode $|C_1^{-1}\psi_1^I|$ and the unstable T-S mode $|\psi_1^I|$ for a Rankine body at the lower branch neutral stability point as a function of A for (*a*) $\epsilon = 0.05$, (*b*) $\epsilon = 0.1$ and (*c*) $\epsilon = 0.2$.

4. Discussion and conclusions

We have formulated a method which uses the PSE to match the asymptotic eigenmodes at the leading edge, formed from the interaction of the free stream with the boundary layer, through the Orr–Sommerfeld region of the body. This method is valid on bodies with a rounded leading edge, where the steady-slip velocity at the edge of the boundary layer has the form

$$U_f = 1 + \frac{\gamma_1}{x_R} + \frac{\gamma_2}{x_R^2} + O\left(x_R^{-3}\right),$$

in the large x_R asymptotic limit, where x_R is a streamwise variable along the surface of the body. We presented lower branch neutral stability point calculations and amplitudes of the unstable T-S mode at this point for a parabolic body and the Rankine body which both satisfy the above property. For the parabolic body, which has a favourable pressure gradient along its surface, we found that the lower branch point was positioned downstream of the flat-plate value as the nose radius of curvature was increased, and the T-S mode amplitude at this point decreased with increasing nose radius. The Rankine body on the other hand has an adverse pressure gradient over most of the body which produces a neutral stability point positioned closer to the nose of the body when compared to the flat-plate value. The unstable T-S mode

amplitude at this point has a double-maximum structure for sufficiently large values of the Reynolds number with both maxima greater than the flat-plate value. However, for smaller Reynolds numbers the T-S mode amplitude decreased from the flat-plate value for increasing nose radius, but still with a second maximum value for larger nose radii.

The present work has revealed how the amplitude of the unstable T-S mode at the lower branch neutral stability point is sensitive to leading edge geometry. This sensitivity is important when determining the position of boundary layer transition. In this paper comparisons with the numerical study of Haddad & Corke (1998) were not possible because the only non-zero nose radius considered by Haddad & Corke corresponds to a Strouhal number $S = 2.3 \times 10^{-3}$, which gives results almost indistinguishable from the flat-plate case (cf. figure 16(*a*) from Haddad & Corke 1998 for a parabola with $S = 2.3 \times 10^{-3}$ with figure 14 from Turner & Hammerton 2006 for a flat plate). A selection of results with larger nose radii using the methods of Haddad & Corke would make an excellent comparison with the parabola results presented in this paper. Although general trends in behaviour have been identified in this paper, the results presented here do not allow a direct comparison with experiments which are typically conducted using modified super ellipses. While the methods of the current paper can be extended to cover analysis of such bodies, a separate receptivity analysis of the leading edge region for the new geometry must be completed in order to describe the transition process.

The writing up of this work took place when the leading author was supported by the EPSRC grant EP/D032202/1. The authors would also like to thank the referees for their comments and suggestions which have improved this paper.

REFERENCES

Andersson, P., Henningson, D. S. & Hanifi, A. 1998 On a stabilization procedure for the parabolic stability equations. *J. Engng Math.* **33** (3), 311–332.

Bertolotti, F. P., Herbert, Th. & Spalart, P. R. 1992 Linear and nonlinear stability of the Blasius boundary layer. *J. Fluid Mech.* **242**, 441–474.

Brown, S. N. & Stewartson, K. 1973 On the propagation of disturbances in a laminar boundary layer. *Proc. Camb. Phil. Soc.* **73**, 493–514.

Chang, C. L. 2003 The Langley stability and transition analysis code (LASTRAC): LST, linear & nonlinear PSE for 2-D, axisymmetric, and infinite swept wing boundary layers. *AIAA Paper* 974, 2003.

Erturk, E. & Corke, T. C. 2001 Boundary layer receptivity to sound at incident angles. *J. Fluid Mech.* **444**, 383–407.

Fuciarelli, D. A., Reed, H. L. & Lyttle, I. 1998 DNS of leading-edge receptivity to sound. *AIAA Paper* 98-2644.

Gaster, M. 1974 On the effects of boundary-layer growth on flow stability. *J. Fluid Mech.* **66**, 465–480.

Goldstein, M. E. 1982 Generation of Tollmien–Schlichting waves by free-stream disturbances at low Mach numbers. *NASA TM 83026*.

Goldstein, M. E. 1983 The evolution of Tollmien–Schlichting waves near a leading edge. *J. Fluid Mech.* **127**, 59–81.

Goldstein, M. E. 1985 Scattering of acoustic waves into Tollmien–Schlichting waves by small streamwise variations in surface geometry. *J. Fluid Mech.* **154**, 509–529.

Goldstein, M. E. & Hultgren, L. S. 1989 Boundary-layer receptivity to long-wave free-stream disturbances. *Annu. Rev. Fluid Mech.* **21**, 137–166.

Goldstein, M. E., Leib, S. J. & Cowley, S. J. 1992 Distortion of a flat-plate boundary layer by free-stream vorticity normal to the plate. *J. Fluid Mech.* **237**, 231–260.

HADDAD, O. M. & CORKE, T. C. 1998 Boundary layer receptivity to free-stream sound on parabolic bodies. *J. Fluid Mech.* **368**, 1–26.

HADDAD, O. M., ERTURK, E. & CORKE, T. C. 2005 Acoustic receptivity of the boundary layer over parabolic bodies at angles of attack. *J. Fluid Mech.* **536**, 377–400.

HAMMERTON, P. W. 1999 Comparison of Lam–Rott and Brown–Stewartson eigensolutions of the boundary-layer equations. *Quart. J. Mech. Appl. Math.* **52** (3), 373–385.

HAMMERTON, P. W. & KERSCHEN, E. J. 1996 Boundary-layer receptivity for a parabolic leading edge. *J. Fluid Mech.* **310**, 243–267.

HERBERT, T. 1993 Parabolized stability equations. *AGARD Rep.,* 4-1–4-34.

KERSCHEN, E. J., CHOUDHARI, M. & HEINRICH, R. A. 1990 Generation of boundary instability waves by acoustic and vortical free-stream disturbances. In *Laminar-Turbulent Transition,* Vol. III, pp. 477–488. Springer.

LAM, S. H. & ROTT, N. 1960 Theory of linearized time-dependent boundary layers. *Cornell University GSAE Rep. AFOSR,* pp. TN-60-1100.

LAM, S. H. & ROTT, N. 1993 Eigen-functions of linearized unsteady boundary layer equations. *J. Fluids Engng* **115**, 597–602.

LANGLOIS, M., CASALIS, G. & ARNAL, D. 1998 On the practical application of the PSE approach to linear stability analysis. *Aerosp. Science Technol.* **2** (3), 167–176.

LIBBY, P. A. & FOX, H. 1963 Some perturbation solutions in laminar boundary-layer theory. Part 1. The momentum equation. *J. Fluid Mech.* **17**, 433–449.

MORKOVIN, M. V. 1985 *Guide to Experiments on Instability and Laminar-Turbulent Transition in Shear Layers*. Notes for AIAA short course.

NICHOLS, D. E. 2001 Boundary layer receptivity of a flat plate with a rounded leading edge. PhD thesis, University of East Anglia, Norwich.

REED, H. L. 1994 Direct numerical simulation of transition: the spatial approach. In Progress in Transition Modelling, *AGARD Rep.* 793. NATO, 6.1–46.

ROSENHEAD 1963 *Laminar Boundary Layers*. Clarendon.

SARIC, W. S. & NAYFEH, A. 1975 Nonparallel stability of boundary-layer flows. *Phys. Fluids* **18**, 945–950.

SARIC, W. S., REED, H. L. & KERSCHEN, E. J. 2002 Boundary-layer receptivity to freestream disturbances. *Annu. Rev. Fluid Mech.* **34**, 291–319.

SARIC, W. S. & WHITE, E. B. 1998 Influence of high-amplitude noise on boundary-layer transition to turbulence. *AIAA Paper* 98-2645.

SMITH, F. T. 1979 On the non-parallel flow stability of the Blasius boundary layer. *Proc. R. Soc. Lond. Ser.* A **366**, 91–109.

TURNER, M. R. 2005 Numerical and asymptotic approaches to boundary-layer receptivity and transition. PhD thesis, University of East Anglia, Norwich.

TURNER, M. R. 2007 Far downstream analysis for the Blasius boundary-layer stability problem. *Quart. J. Mech. Appl. Math.* **60** (3), 255–274.

TURNER, M. R. & HAMMERTON, P. W. 2006 Asymptotic receptivity analysis and the parabolized stability equation: a combined approach to boundary layer transition. *J. Fluid Mech.* **562**, 355–381.

WANDERLEY, J. B. V. & CORKE, T. C. 2001 Boundary layer receptivity to free-stream sound on elliptic edges of flat plates. *J. Fluid Mech.* **429**, 1–21.